nature structural & molecular biology

Diversity of chemical mechanisms in thioredoxin catalysis revealed by single-molecule force spectroscopy

Raul Perez-Jimenez[1], Jingyuan Li[2], Pallav Kosuri[1,3], Inmaculada Sanchez-Romero[4], Arun P Wiita[1], David Rodriguez-Larrea[4], Ana Chueca[5], Arne Holmgren[6], Antonio Miranda-Vizuete[7], Katja Becker[8], Seung-Hyun Cho[9], Jon Beckwith[9], Eric Gelhaye[10], Jean P Jacquot[10], Eric Gaucher[11], Jose M Sanchez-Ruiz[4], Bruce J Berne[2] & Julio M Fernandez[1]

Thioredoxins (Trxs) are oxidoreductase enzymes, present in all organisms, that catalyze the reduction of disulfide bonds in proteins. By applying a calibrated force to a substrate disulfide, the chemical mechanisms of Trx catalysis can be examined in detail at the single-molecule level. Here we use single-molecule force-clamp spectroscopy to explore the chemical evolution of Trx catalysis by probing the chemistry of eight different Trx enzymes. All Trxs show a characteristic Michaelis-Menten mechanism that is detected when the disulfide bond is stretched at low forces, but at high forces, two different chemical behaviors distinguish bacterial-origin from eukaryotic-origin Trxs. Eukaryotic-origin Trxs reduce disulfide bonds through a single-electron transfer reaction (SET), whereas bacterial-origin Trxs show both nucleophilic substitution (S_N2) and SET reactions. A computational analysis of Trx structures identifies the evolution of the binding groove as an important factor controlling the chemistry of Trx catalysis.

Enzymes are exceptional catalysts that can accelerate reaction rates by several orders of magnitude[1]. However, little is known about how enzymes developed their chemical mechanisms to obtain high reaction rates and specificity. The mechanisms of numerous enzymatic reactions have been studied using protein biochemistry and structural biological techniques such as X-ray crystallography and NMR[2,3]. These studies have been useful in identifying many structural features and conformational changes necessary for the catalytic activity of enzymes. Nonetheless, the dynamic sub-Ångström–scale rearrangements of the participating atoms necessary for catalysis cannot be detected by these techniques. Recently developed single-molecule techniques have shown promise in uncovering the dynamics of enzymatic activity at a length scale that was previously impossible to observe. For example, both optical tweezers and fluorescence techniques have been used extensively to detect the motions of molecular motors, a large class of ATP-consuming, force-generating enzymes[4,5].

In this work, we use single-molecule force-clamp spectroscopy techniques to investigate the chemical mechanisms of catalysis of disulfide-reducing enzymes—Trxs. These oxidoreductases are present in all known organisms from bacteria to humans. Trxs posses a highly conserved active site (CXXC) that catalyzes the reduction of target disulfide bonds, which are involved in a multitude of cellular processes[6,7]. Several methods based on spectrophotometry have been used widely to determine the activity of Trxs, including monitoring of oxidation of NADPH in the presence of Trx reductase (TxrR) or ribonucleotide reductase[8,9], observation of the turbidity of solutions containing insulin, which readily aggregates after reduction of its disulfide bonds[9], and the use of Ellman's reagent (DTNB), where reduction by thiol groups generates products that can be easily detected with a spectrophotometer[6]. The change in tryptophan fluorescence has also been used to measure rates of Trx oxidation and reduction[10]. Although highly effective in monitoring the overall activity of Trx enzymes, these methods do not probe the chemical mechanisms underlying the catalytic activity of these enzymes.

Recent single-molecule force-spectroscopy experiments have demonstrated that the application of a mechanical force to a substrate disulfide bond can regulate the catalytic activity of Trxs[11], revealing different chemical mechanisms of reduction that can be readily distinguished by their sensitivity to an applied force. A simple form of catalysis in *Escherichia coli* Trx corresponded to a straightforward S_N2-type chemical reaction characterized by an exponential increase of the rate of reduction with the pulling force[12,13]. This S_N2-type reaction

[1]Department of Biological Sciences, [2]Department of Chemistry, and [3]Department of Biochemistry and Molecular Biophysics, Columbia University, New York, New York, USA. [4]Facultad de Ciencias, Departamento de Química-Fisica, Universidad de Granada, Granada, Spain. [5]Estación Experimental del Zaidin, CSIC, Granada, Spain. [6]Medical Nobel Institute for Biochemistry, Department of Medical Biochemistry and Biophysics, Karolinska Institutet, Stockholm, Sweden. [7]Centro Andaluz de Biología del Desarrollo (CABD-CSIC), Departamento de Fisiología, Anatomía y Biología Celular, Universidad Pablo de Olavide, Sevilla, Spain. [8]Interdisciplinary Research Center, Justus Liebig University, Giessen, Germany. [9]Department of Microbiology and Molecular Genetics, Harvard Medical School, Boston, Massachusetts, USA. [10]Nancy University, IFR110 GEEF, UMR 1136 Interactions Arbres Microorganismes, Faculte des Sciences, Vandoeuvre Cedex, France. [11]Georgia Institute of Technology, School of Biology, Atlanta, Georgia,USA. Correspondence should be addressed to R.P.-J. (raulpjc@biology.columbia.edu) or J.M.F. (jfernandez@columbia.edu).

Received 12 February; accepted 27 May; published online 13 July 2009; doi:10.1038/nsmb.1627

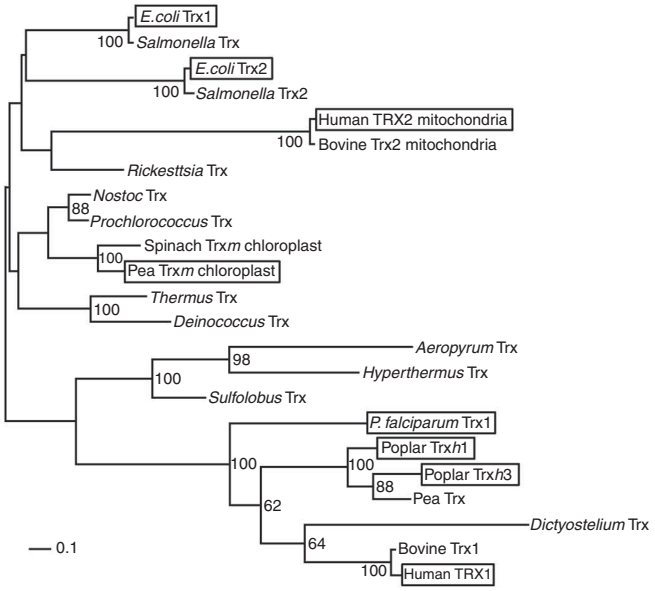

Figure 1 Phylogeny of Trx homologs from representative species of the three domains of life. Branch lengths were estimated using maximum likelihood, with rate variation modeled according to a gamma distribution. Scale bar represents amino acid replacements per site per unit of evolutionary time. Posterior probabilities are shown at nodes of the phylogeny when greater than 50%. The lack of strong node supports deep in the phylogeny results from the ambiguous placement of mitochondrial sequences, possibly resulting from long-branch attraction effects with nonbacterial sequences. In contrast, there is strong support for the grouping of chloroplast and cyanobacteria (not shown). Boxes highlight the proteins studied experimentally in this work.

was absent in human Trx, which instead uses a force-independent disulfide-reduction mechanism. An additional chemical mechanism of reduction was characterized by its rapid inhibition by a force applied to the substrate disulfide bond. This chemical mechanism is unique to disulfide bond reduction catalyzed by Trx enzymes, and it was explained by a Michaelis-Menten type reaction in which the binding of the enzyme to the stretched polyprotein and the subsequent structural organization of the participating sulfur atoms precede the chemical reaction.

Thus, the single-molecule reduction assay that we have previously developed can distinguish the chemistry of a simple S_N2 reaction from the more elaborate pathways for the reduction of disulfide bonds that are unique to Trx enzymes. It is of interest, then, to consider the application of these sensitive single-molecule techniques to study the evolution of chemical mechanisms in this family of enzymes. The simplest evolutionary hypothesis is that the ancient forms of Trx had capabilities that were comparable to those of simple reducing agents. Evolutionary pressures then drove the enzymes toward developing unique and more efficient mechanisms of reduction. As a first step toward understanding the evolution of Trx chemistry, we have applied the single-molecule assay to examine the chemical mechanisms of reduction of a sample of eight extant Trx enzymes covering four kingdoms of life. From this analysis, we report several new advances. First, we demonstrate that the differences in the chemical mechanisms of reduction between *E. coli* Trx and human TRX1 (also known as TXN), which we have reported previously, can now be generalized to enzymes of bacterial-origin versus those of eukaryotic-origin. We also demonstrate a third mechanism for disulfide bond reduction that corresponds to a single-electron transfer reaction and that is present in all Trx enzymes. Finally, through a computational analysis of Trx structures, we show that the changes in the catalytic chemistry correlate well with a deepening of the binding grove observed in Trxs of eukaryotic origin. These last results identify the evolution of the binding groove as an important structural adaptation controlling the chemistry of disulfide reduction in the Trx family of enzymes.

RESULTS

Selection of Trxs from different species

To investigate the various catalytic mechanisms developed by Trx, we have selected of a set of Trxs belonging to a representative group of species from different kingdoms: Animalia, Eubacteria, Protista and Plantae (covering two domains of life: bacteria and eukaryotes). Trx is widely distributed in all living organisms from bacteria to mammals. In addition, the existence of a second paralogous Trx gene (*Txn2*) seems to be common in animals, protists and Gram-negative bacteria[14–18]. In protists and animals, Trx1 is located in the cytoplasm, whereas Trx2 is present in mitochondria[18,19]. Notably, mitochondrial Trx2 from mammals has been shown to have higher similarity with *E. coli* Trx1 than with cytosolic Trx1 from mammals[16]. In the case of plants, a rich variety of Trx genes can be found encoding more than 20 different types of Trxs[20] that are classified into six isoforms: Trx*f*, *h*, *m*, *x*, *y* and *o*. The *f*, *m*, *x* and *y* forms are plastidic Trxs, *h* forms are mainly cytosolic and *o* forms are found in mitochondria[21]. In this study, we have included both human cytosolic and mitochondrial Trxs from animals, poplar Trx*h*1 (featuring a CPPC active site instead of the canonical CGPC), poplar Trx*h*3 and pea chloroplastic Trx*m* from plants, *E. coli* Trx1 and Trx2 from bacteria and, finally, *Plasmodium falciparum* (malaria parasite) Trx1 from protists.

A sequence alignment of the Trxs of interest shows that the residues around the active site are highly conserved (**Supplementary Fig. 1**). The construction of a phylogenetic tree (**Fig. 1**), incorporating additional Trxs from the three domains of life, classifies *E. coli* Trx1 and Trx2, human TRX2 and pea Trx*m* as 'bacterial-type' Trxs (upper branches in **Fig. 1**) and human TRX1, poplar Trx*h*1 and Trx*h*3 and *P. falciparum* Trx1 as 'eukaryotic-like' Trxs (lower branches in **Fig. 1**). The construction of a larger tree incorporating more than 200 Trx sequences (not shown) corroborates the suggestion that the sequences used are widely distributed and that they are representative for the entire Trx family.

Force-dependent chemical kinetics of disulfide reduction

As in our previous work, we have used an atomic force microscope in its force-clamp mode to study the chemistry of disulfide reduction by Trx[11,22]. Briefly, we chose for a substrate a polyprotein composed of eight domains of the 27th module of human cardiac titin, in which each module contains an engineered disulfide bond between the 32nd and 75th positions $(I27_{G32C\text{-}A75C})_8$ (ref. 11). By our method, the first pulse of force (175 pN, 0.3 s) applied to the polyprotein allows the rapid unfolding of the $I27_{G32C\text{-}A75C}$ modules up to the disulfide bond. The individual unfolding events can be registered as steps of $\sim$10.5 nm per module. After the first pulse, the disulfide bonds become exposed to the solvent, where the Trx molecules are present in the reduced form owing to the presence of Trx reductase and NADPH (Trx system)[6]. A second pulse of force is applied to monitor single disulfide reductions by Trx enzymes, recorded as a second series of steps of $\sim$13.5 nm per domain (**Fig. 2a,b**). We have accumulated several traces per force (15–50), which have been averaged and fit with a single exponential with a time constant τ (**Fig. 2c,d**). We thus obtain the reduction rate at a given force ($r = 1/\tau$).

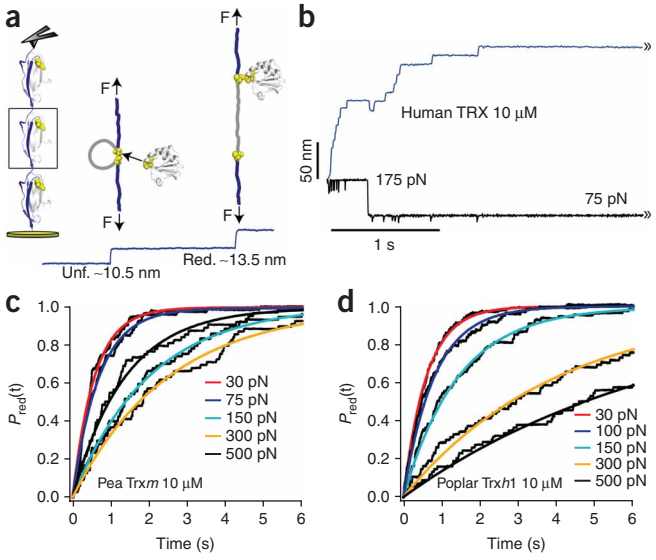

Figure 2 Single-molecule force-clamp detection of disulfide bond–reduction events catalyzed by Trx enzymes. (**a**) Graphic representation of the force-clamp experiment. A first force pulse rapidly unfolds (Unf.) the I27 modules of a polyprotein, exposing the buried disulfide bonds to the solvent. A second force pulse monitors single disulfide-reduction events (Red.) that are uniquely identified by the extension of the residues trapped behind the disulfide bond. (**b**) Trace showing the unfolding and consequent disulfide reductions of a $(I27_{G32C-A75C})_8$ polyprotein. In the example shown, the unfolding pulse was set at 175 pN for 0.3 s, and the reduction pulse was set to 75 pN for several seconds. (**c**,**d**) Probability of reduction ($P_{red}(t)$) obtained by summing and normalizing traces of disulfide bond reductions at different forces (second pulse) for pea Trx*m* (10 μM) (**c**) and for poplar Trx*h*1 (10 μM) (**d**). The smooth curves are single-exponential fits to $P_{red}(t)$ from which we measure the rate of reduction as $r = 1/\tau$, where τ is the time constant measured by the fits at each given force.

We have applied our single-molecule assay to obtain the force-dependency of the rate of reduction by the selected Trxs (**Fig. 3**). From these data we can readily distinguish three different types of force-dependencies. First, all tested Trx enzymes showed a negative force-dependency in the range 30–200 pN. Second, all Trx enzymes from bacterial origin show that, after reaching a minimum rate at around 200 pN, the rate of reduction increases exponentially at greater forces. Third, at forces greater than 200 pN, enzymes from eukaryotic origin show a rate of reduction that becomes force-independent. Therefore, our previous observations in *E. coli* and human TRXs can now be generalized to bacterial-origin and eukaryotic-origin Trxs.

We have previously proposed that the reduction mechanism observed when the substrate is stretched at low forces (30–200 pN) is similar to a Michaelis-Menten (MM-S_N2) reaction in which the formation of an enzyme-substrate complex is determinant[11]. Upon binding, the substrate disulfide bond needs to rotate to achieve the correct geometry necessary for an S_N2 reaction to occur, that is, the three involved sulfur atoms form an $\sim 180^\circ$ angle[11,22,23]. This rotation causes the shortening of the substrate polypeptide along the stretching force axis, as determined by the negative value of Δx_{12} in our kinetic model (**Table 1**, **Fig. 4** and **Supplementary Fig. 2**). This mechanism is rapidly inhibited as the force increases, generating the negative dependence of the reduction rate with the pulling force in all Trx enzymes (**Fig. 3**). Here we demonstrate that, whereas the absolute rate of reduction varies from enzyme to enzyme, the general characteristics of this mechanism of reduction are apparent in all of them.

According to the parameters obtained from the fit of the data to a simple MM-S_N2–type kinetic model (**Table 1**), we found that an extrapolation to zero force predicts rate constants ranging from 1.2×10^5 M^{-1} s^{-1} for poplar Trx*h*3 to 6.5×10^5 M^{-1} s^{-1} for human TRX2. These values are markedly similar to those obtained previously using insulin disulfides as substrates and *E. coli* Trx[8]. The value of Δx_{12} remained below 1 Å, except for *E. coli* Trx2 and poplar Trx*h*3, which gave values of more than 1 Å (**Table 1**). These high values of Δx_{12} represent a higher rotation angle of the substrate disulfide bond for the S_N2 reaction[22]. This mechanism is unique to Trx enzymes, and it seems to be the result of evolutionary pressure toward developing an efficient mechanism of disulfide reduction that is not possible with simple chemical reagents[12].

When forces of more than 200 pN were applied to the substrate, the MM-S_N2 mechanism was blocked, and a second force-dependent mechanism of reduction became dominant. This was true for all types of Trx enzymes that we tested. In enzymes of bacterial origin, this high-force mechanism (**Fig. 3a**) seems to be analogous to that of simple chemical compounds such as cysteine, glutathione or DTT, which reduce disulfide bonds through a force-dependent S_N2 thiol-disulfide exchange reaction with bond elongation at the transition state[12,13]. We incorporated this reaction into our kinetic model (k_{02}),

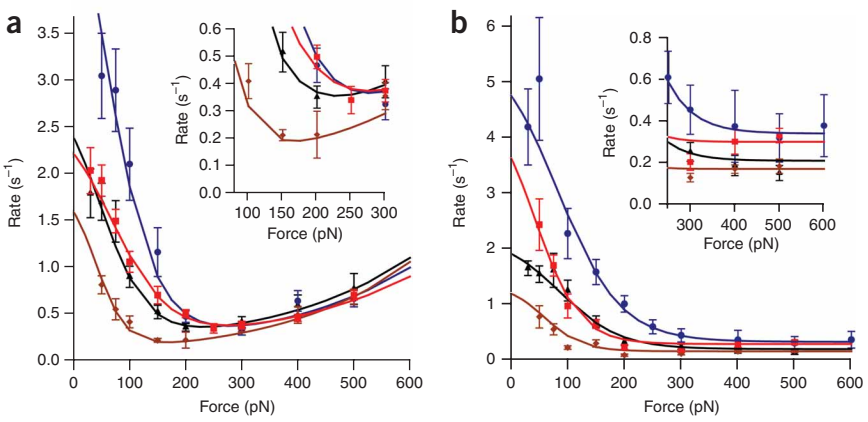

Figure 3 Force-dependency of the rate of disulfide reduction by Trx enzymes from different species. (**a**) Bacterial-origin Trxs: human mitochondrial TRX2 (blue), *E. coli* Trx1 (red), pea chloroplastic Trx*m* (black) and *E. coli* Trx2 (brown). Whereas the Michaelis-Menten (low-force) mechanism differs in magnitude among the Trxs, the simple S_N2-like reaction observed at higher forces is similar in all of them. Inset, a magnified view of the traces in the region where they reach a minimum. (**b**) Eukaryotic-origin Trxs: human TRX1 (blue; data from ref. 11), *Plasmodium* Trx (red), poplar Trx*h*1 (black) and poplar Trx*h*3 (brown). The most noticeable feature is the absence of the S_N2-like reaction at high forces in all eukaryotic Trxs. Inset, an expansion of the minimum rate of reduction attained at high forces. In all experiments the concentration of Trx was 10 μM. The smooth lines are fits of the kinetic model described in the **Supplementary Methods**. The kinetics parameters obtained are summarized in **Table 1**. The error bars are given by the s.e.m. obtained by the bootstrap method.

Table 1 Kinetic parameters for Trx enzymes from different species

	α_0 (μM^{-1} s^{-1})	β_0 (s^{-1})	γ_0 (μM^{-1} s^{-1})	k_{10} (s^{-1})	Δx_{12} (Å)	Δx_{02} (Å)	λ_0(s^{-1})
E. coli Trx1	0.25 ± 0.02	24 ± 2	0.012 ± 0.002	4.7 ± 0.5	−0.75 ± 0.05	0.16 ± 0.01	0.08 ± 0.02
E. coli Trx2	0.18 ± 0.04	23 ± 3	0.009 ± 0.002	4.5 ± 0.5	−1.41 ± 0.03	0.19 ± 0.01	0.07 ± 0.03
Human TRX2	0.65 ± 0.15	25 ± 2	0.019 ± 0.004	3.8 ± 0.6	−0.84 ± 0.05	0.19 ± 0.02	0.06 ± 0.04
Pea Trx*m*	0.28 ± 0.03	22 ± 2	0.012 ± 0.002	5.0 ± 0.6	−0.93 ± 0.08	0.17 ± 0.02	0.09 ± 0.04
P. falciparum Trx1	0.43 ± 0.05	25 ± 2	–	4.8 ± 0.5	−1.01 ± 0.05	–	0.34 ± 0.02
Human TRX1	0.52 ± 0.05	33 ± 2	–	3.1 ± 0.9	−0.71 ± 0.05	–	0.35 ± 0.02
Poplar Trx*h*3	0.12 ± 0.03	30 ± 3	–	4.4 ± 0.4	−1.16 ± 0.08	–	0.17 ± 0.02
Poplar Trx*h*1	0.22 ± 0.02	28 ± 3	–	5.5 ± 0.6	−0.68 ± 0.07	–	0.17 ± 0.03

The parameters were obtained using the kinetic model described in the **Supplementary Methods**. They are the result of numeric optimization of the global fit using the downhill simplex method.

obtaining a value for the elongation of the disulfide bond at the transition state of ~0.18 Å (Δx_{02} in **Table 1**), a value that is similar to those obtained when using cysteine as a nucleophile (~0.2 Å)[12]. Absence of the S_N2-like mechanism seems to be common to all eukaryotic-origin Trx, where the rate of the reaction became force-independent at greater forces (**Fig. 3b**). We measured this force-independent mechanism as a constant rate of reduction that ranged from 0.2 s^{-1} to 0.4 s^{-1} (**Fig. 3b**, inset). We speculate that in enzymes of bacterial origin the minimum value of the reduction rate is also limited by this force-independent 'floor' in the rate of reduction, which varies in the range 0.2–0.4 s^{-1} (**Fig. 3a**, inset). We incorporated this mechanism into our kinetic model in the form of a constant parameter, λ (see kinetic model in **Supplementary Fig. 2** and **Supplementary Methods**), which contributes equally to the reduction rate throughout the entire range of forces (**Table 1**).

An interesting possibility that may explain this force-independent chemical mechanism is a SET reaction via tunneling, a process that has been observed in enzymes containing metallic complexes[3,24]. In addition, it has been suggested that SET reactions are highly favored when steric hindrance occurs[25]. To test whether an electron transfer mode of reduction would be force-independent, we investigated the kinetics of disulfide reduction under force by a metal. Some metals participate in oxidation-reduction processes in proteins via electron-transfer reactions that are governed by the reduction potential[26,27]. We studied experimentally the reduction of disulfide bonds by zinc nanoparticles (diameter <50 nm)[28]. In sharp contrast to all other reducing agents that we studied, the rate of reduction of disulfide bonds by zinc was force-independent (**Fig. 4a**). Owing to the experimental difficulty of working at low forces with zinc nanoparticles, we included only experiments done using forces of more than 200 pN. Our results support the idea that the force-independent mechanism is a barrier-free electron-tunneling reaction that does not require the precise orientation for the S_N2 reaction.

Another piece of evidence in support of the SET mechanism can be obtained from the analysis of the concentration-dependencies of the MM-S_N2 and SET reduction mechanisms. We measured reduction kinetics by human TRX1 at different forces and concentrations (50–600 pN and 2–15 μM of TRX1) and found that the low-force MM-S_N2 mechanism (50–200 pN) is clearly dependent on the concentration of the enzyme, whereas the high-force SET mechanism (>300 pN) is essentially concentration-independent (**Supplementary Fig. 3**). As expected for a first-order MM-S_N2 mechanism, where substrate binding to the groove is determinant, the rate of reduction showed linear concentration-dependence when working below saturating concentrations of TRX1 enzyme (<15 μM)[11]. However, given that the TRX1 and NADPH system was in equilibrium owing to the presence of TrxR[29,30], the redox potential of TRX1 would be expected to remain constant (from the Nernst equation). Therefore, the potential difference between TRX1 and substrate, and thus the rate of electron transfer[31], would also be constant in this TRX1 concentration range. Hence, the SET mechanism should be essentially independent of the enzyme concentration[32,33]; this is verified in **Supplementary Fig. 3**.

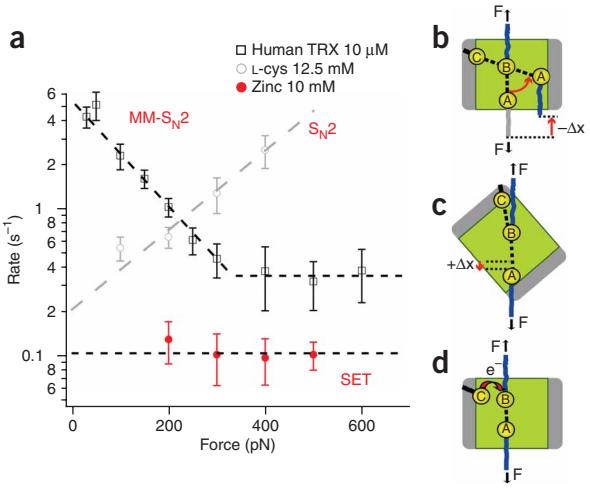

Figure 4 The three chemical mechanisms of disulfide reduction detected by force-clamp spectroscopy. (**a**) Force-dependency of the rate of reduction of disulfide bonds by different reducing agents. Human TRX1 (black squares; data from ref. 11) shows the characteristic enzymatic mechanism of reduction, marked by a negative force-dependency that reaches a force-independent minimum. L-cysteine (gray circles; data from ref. 12) shows the characteristic S_N2-like mechanism marked by an exponential increase in the rate of reduction with the applied force. Finally, metallic zinc (red circles) demonstrates a reduction mechanism that seems to be force-independent. Bacterial Trx enzymes make use of all three mechanisms. (**b**) Schematic representation of the Michaelis-Menten reduction mechanism present in all Trx enzymes. The substrate disulfide bond is shown in the binding groove of the enzyme. Rotation of the substrate disulfide bond against the pulling force is required for the 180° alignment with the catalytic cysteine and for reduction to occur. (**c**) We speculate that the simple S_N2-like mechanism observed at high forces results from aligning the substrate disulfide bond with the catalytic cysteine, without entering the binding groove. This conformation is favored by a shallow binding groove, allowing for the simple S_N2-type lengthening of the substrate disulfide bond at the transition state, which is the origin of the exponential dependency of the rate of reduction. (**d**) Representation of the single-electron transfer (SET) mechanism that is ubiquitous to all Trxs. This mechanism can occur irrespective of the orientation of the disulfide bond and is more visible in eukaryotic Trxs at high forces.

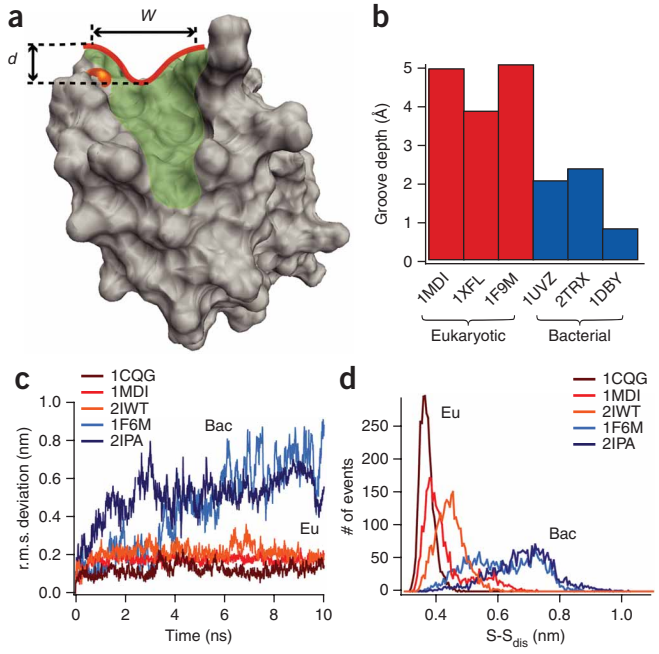

Figure 5 Structural analysis and molecular dynamics simulations of the binding groove in Trx enzymes. (**a**) Geometric dissection of the hydrophobic binding groove, shaded in green and outlined in red for human TRX1 (PDB 3TRX[48]). The depth and width of the binding groove in the region surrounding the catalytic cysteine are indicated by arrows, and the active cysteine is colored orange. (**b**) Groove depth for three eukaryotic-origin Trxs (red)—human TRX1 (PDB 1MDI[49]); *A. thaliana* Trx*h*1 (PDB 1XFL[50]) and spinach Trx*f* (PDB 1F9M[51])—and three bacterial-origin Trxs (blue)—human TRX2 (PDB 1UVZ[52]); *E. coli* Trx1 (PDB 2TRX[53]) and *C. reinhardtii* Trx*m* (PDB 1DBY[54]). It is clear that the eukaryotic binding grooves are deeper than their bacterial counterparts. (**c**) Molecular dynamics simulation of the substrate mobility within the binding groove for different eukaryotic (Eu, red) and bacterial (Bac, blue) Trxs. Three eukaryotic complexes were used: human TRX with the substrate REF-1 (PDB 1CQG[55]); human TRX1 with NF-κB (PDB 1MDI[49]) and barley Trx*h*2 with protein BASI (PDB 2IWT[34]). The two bacterial complexes were *E. coli* Trx1 with Trx reductase (PDB 1F6M[36]) and *B. subtilis* Trx bound to ArsC (PDB 2IPA[35]). The large r.m.s. deviation of the bacterial Trxs (blue) indicates a high substrate mobility which may facilitate collisions orientated so as to favor S_N2 reactions. Eukaryotic Trxs (red) are highly restricted, which may explain the different chemical behavior at high forces as compared to bacterial Trxs (**Fig. 3**). (**d**) Diatomic distance distribution of the disulfide bond (S-S_{dis}) in the Trx-substrate mixed intermediate, using the same structures as in **c**. Again, we infer higher mobility of the substrate in bacterial-origin Trxs, as indicated by the broader distance distributions of the bacterial complexes (blue) as compared to those of eukaryotic Trxs (red).

Our results suggest that there are three distinct mechanisms of reduction that operate simultaneously in a Trx enzyme. These mechanisms are identified by their force-dependency, as shown in **Figure 4**. The most complex mechanism is characterized by a negative force-dependency and is unique to enzymatic catalysis by Trx (**Fig. 4a**,**b**). This enzymatic mechanism of reduction is characterized by a MM-S_N2 reaction between the substrate polypeptide and the binding groove of the enzyme, followed by a rotation of the substrate disulfide bond to gain position for the S_N2 reduction mechanism[11,22] (**Fig. 4a**,**b**). A much simpler mechanism is that of a regular S_N2 reaction, characterized by a rate of reduction that increases exponentially with the applied force. This mechanism is well represented by nucleophiles such as L-cysteine (**Fig. 4a**), glutathione and DTT[11,12]. By this mechanism, the substrate disulfide bond and the catalytic cysteine of the enzyme orient themselves with the pulling force, without needing a rotation of the substrate disulfide bond (**Fig. 4c**). We suspected that this mechanism would be possible only if the Trx enzyme had a shallow binding grove that allowed many other orientations of the substrate-enzyme complex. Finally, the third mechanism is the force-independent, barrier-free electron-tunneling transfer mechanism, revealed by the action of metallic zinc (**Fig. 4d**). It is inevitable that, if the disulfide bond gets close enough to the thiolate anion of the catalytic cysteine, the electron tunneling will occur, albeit at a low rate.

Thus, comparing the data in **Figures 3** and **4**, it is clear that the main difference between enzymes of bacterial and eukaryotic origin is the elimination of the high-force, simple S_N2-like mechanism of reduction. We speculate that this drastic change in the catalytic chemistry would be caused by changes in the structure of the enzyme as it evolved. The most salient feature in the structure of Trx enzymes is the binding groove into which the target polypeptide first binds, to be subsequently reduced by the exposed thiol of the catalytic cysteine (**Fig. 5a**).

Structural analysis and molecular dynamics simulations

To study the role of the structure in the chemical behavior of Trxs, we analyzed the structure of the binding groove of a set of bacterial-origin and eukaryotic-origin Trxs. We studied three eukaryotic-origin enzymes—human TRX1, *Arabidopsis thaliana* Trx*h*1 and spinach Trx*f*—and three bacterial-origin enzymes—human mitochondrial TRX2, *E. coli* Trx1 and *Chlamydomonas reinhardtii* Trx*m*. From the X-ray or NMR structures, we defined structural axes that allowed us to calculate the depth and width of the binding groove in the region surrounding the catalytic cysteine (**Fig. 5a** and **Supplementary Methods**). We found that eukaryotic Trx enzymes have binding grooves that are several angstroms deeper than those of bacterial origin (**Fig. 5b**). By contrast, the width of the binding groove remained the same (**Supplementary Fig. 4**).

We explored the consequences of a deepening binding groove using molecular dynamics simulations to probe the mobility of a bound polypeptide (see **Supplementary Methods** for computational procedures). For these simulations, we considered a set of enzyme structures obtained with mixed disulfide intermediates between the catalytic cysteine and a cysteine in the bound substrate. Such structures capture the general disposition of the substrate in the catalytic site of the Trx enzyme. We used three eukaryotic complexes—human TRX1 with the substrate REF-1, human TRX1 with NF-κB and barley Trx*h*2 with protein BASI—and two bacterial complexes—*E. coli* Trx1 with Trx reductase and *B. subtilis* Trx with ArsC complex. To compare these structures, we took into account 13 residues of the substrates, with the binding cysteine always set as the seventh residue. For the molecular dynamics simulations, we removed the substrate-enzyme disulfide bond to allow substrate mobility. The shallow binding groove of bacterial Trxs allows the substrate to be mobile (**Fig. 5c**). By contrast, the deeper groove found in Trx enzymes of eukaryotic origin tends to freeze the substrate into a much smaller range of conformations. Similarly, the measured distribution of the distances between the reacting sulfur atoms is smaller and more narrowly distributed in the deeper binding groove of Trx enzymes of eukaryotic origin than in those with the shallower grooves found in enzymes of bacterial origin (**Fig. 5d**).

As an additional test, we carried out molecular dynamics simulations in which the substrate was removed from the Protein Data Bank structures for two Trx complexes: one from eukaryotic origin, barley

Trx*h*2 with protein BASI (PDB 2IWT[34]), and the other from bacterial origin, *B. subtilis* Trx with ArsC complex (PDB 2IPA[35]). We found no appreciable difference in the dynamics of the groove between the bacterial and the eukaryotic Trxs (**Supplementary Fig. 5**). In fact, the averaged value of the r.m.s. deviation difference is 0.035 ± 0.028 for PDB 2IWT and 0.023 ± 0.031 for PDB 2IPA (the error indicates s.d.). These results support the idea that the large differences in the mobility of the substrate that we report (**Fig. 5c**,**d**) are due to the different binding constraints of the groove.

Finally, we compared the *B*-factor distribution of the substrate from the PDB structures. The *B*-factors of protein crystal structures reflect the fluctuation of atoms around their average positions and provide information about protein dynamics. In particular, we compared the *B*-factors of eukaryotic barley Trx*h*2 bound to protein BASI (PBD 2IWT) with that of *E. coli* Trx bound to Trx reductase (PDB 1F6M[36]), both from X-ray crystallographic experiments (**Supplementary Fig. 6**). Consistent with our simulation results (**Fig. 5c**), the substrate in 1F6M (bacterial-origin Trx) has larger *B*-factors than does eukaryotic Trx 2IWT.

These structural observations suggest that a major feature in the evolution of Trx enzymes has been an increase in the depth of the binding groove, increasing the efficiency of the MM-S_N2 mechanism and eliminating the simple S_N2 mechanism of catalysis.

DISCUSSION

Over the past 4 billion years, the chemistry of living organisms has changed continuously in response to changes in atmospheric conditions and biological phenomena. For example, the large increase in the level of atmospheric oxygen that occurred about ~2.5 billion years ago is thought to have triggered a chemical expansion[37,38] that had a large impact on the chemistry of enzymatic reactions, especially those involving redox transformations[38,39]. However, understanding how enzymes have adapted their chemical mechanisms to evolutionary pressures remains a challenge in molecular biology.

Here we show that single-molecule force-clamp spectroscopy can be a valuable tool to examine the evolution of Trx catalysis by studying the chemistry of eight Trx enzymes from four different kingdoms. We show that three different chemical mechanisms for disulfide reduction can be distinguished in Trx enzymes by their sensitivity to a mechanical force applied to their substrate. Common to all Trx enzymes is a highly efficient Michaelis-Menten–type mechanism of disulfide bond reduction, characterized by a negative force-dependency (**Fig. 4a**,**b**). Also common to all enzymes is a low-rate, force-independent mechanism of reduction that, owing to its similarity to metallic zinc, may be due to a barrier-free electron-tunneling mechanism (**Fig. 4a**,**d**). Finally, enzymes of bacterial origin show an additional mechanism of reduction, comparable to that of a simple S_N2 reaction and showing a force-dependency similar to that of glutathione or cysteine[12,13] (**Fig. 4a**,**c**). This simple S_N2 mechanism seems to have been eliminated from Trx enzymes of eukaryotic origin, suggesting that the mechanism of disulfide bond reduction by Trx enzymes was altered at an early stage of eukaryotic evolution.

We identify the physical characteristics of the binding groove as important factors in the evolution of Trx catalysis. The appearance of the hydrophobic binding groove allowed Trxs to bind the substrate in a specific fashion, generating a stabilizing interaction that allows the enzyme to regulate the geometry and orientation of the substrate disulfide bond in the catalytic site of the enzyme. This binding mechanism results in the Michaelis-Menten–type kinetics of reduction observed in all Trx. It is noteworthy that, as the binding groove deepens in enzymes of eukaryotic origin, the S_N2-like mechanism of reduction disappears. These observations are in agreement with the view that the S_N2-like mechanism of reduction observed in bacterial Trx enzymes results from less specific enzyme-substrate interactions (**Fig. 4c**). The emergence of eukaryotes gave rise to vastly more complex biological systems, resulting in a myriad of new functions and targets[40]. It is tempting to speculate that the deepening of the binding groove in eukaryotic Trx (**Fig. 5**) may have been an important structural adaptation that improved the specificity of substrate-enzyme interactions.

However, evolutionary optimization of Trx activity is clearly a much more complex multiparameter function involving other structural features and cofactors. Most importantly, Trxs work together with TrxRs, which convert oxidized Trx to its active dithiol form. There are major differences in the structure and mechanism of TrxR across the evolutionary tree, and it is reasonable to consider that the evolution of the chemical mechanisms found in Trx has been tightly associated with the evolution of TrxR. In our experiments we have used generic bacterial and eukaryotic TrxR to keep the Trx enzymes in the reduced state. We anticipate that our assay can be expanded by contrasting the effect of different TrxR enzymes in the observed chemistry of Trx.

From a biological point of view, an interesting hypothesis is that the simple S_N2-like mechanism present in bacterial Trxs might be related to their ability to live in extreme environments, where elevated mechanical forces might result as a consequence of the high pressures or extreme salinity that cause cells to swell or shrink[41–43]. As we have shown here, under such conditions the enzymatic Michaelis-Menten–type mechanism of reduction would become inoperative. In support of this view, Trx has been shown to promote high-pressure resistance in *E. coli*[44].

Our work generally demonstrates the usefulness of combining single-molecule force spectroscopy together with molecular dynamics simulations in probing enzymatic chemistry. We observe substantial differences in the chemical mechanisms of extant Trx enzymes. It would be interesting to track the evolution of these chemical mechanisms using resurrected ancient Trx enzymes. Owing to an extensive sequence database and the development of sophisticated maximum-likelihood algorithms for the reconstruction of ancient DNA sequences[45], reconstructing the evolution of chemical mechanisms in this class of important enzymes now seems entirely plausible. We anticipate that the enzymatic studies carried out on Trx at the single-molecule level can serve as a starting point to investigate the chemistry of other enzymes, such as C-S lyases[46] or proteases[47], for which the catalyzed rupture of covalent bonds is the fundamental process.

METHODS

Methods and any associated references are available in the online version of the paper at http://www.nature.com/nsmb/.

Note: Supplementary information is available on the Nature Structural & Molecular Biology website.

ACKNOWLEDGMENTS

We thank S. Garcia-Manyes and J. Morrone assistance in writing the manuscript and all the Fernandez laboratory members for helpful discussions. This work was supported by the US National Institutes of Health grants HL66030 and HL61228 to J.M.F., grant GMO55090 to J.B., grant GM43340 to B.J.B., grant I.C.E. (Columbia University) to B.J.B. and J.M.F., grant BIO2006-07332 from the Spanish Ministry of Education and Science and FEDER Funds to J.M.S.-R.

AUTHOR CONTRIBUTIONS

R.P.-J., J.L. and J.M.F. designed the research; R.P.-J., J.L., P.K., I.S.-R. and A.P.W. carried out the experiments; R.P.-J., J.L., P.K., I.S.-R. and J.M.F. conducted the

data analysis; D.R.-L. and J.M.S.-R. provided Trx from *E. coli*; A.C. provided Trx*m* from pea; A.H. provided human TRX1; A.M.-V. provided human TRX2; K.B. provided Trx1 from *P. falciparum*; S.-H.C. and J.B. provided Trx2 from *E. coli*; E. Gelhaye and J.P.J. provided Trx*h*1 and Trx*h*3 from poplar; R.P.-J. and E. Gaucher performed the phylogenetic analysis; J.L. and B.J.B. performed computational analysis and molecular dynamics simulations; R.P.-J., J.L., P.K. and J.M.F. wrote the paper; all authors have actively participated in revising the manuscript.

Published online at http://www.nature.com/nsmb/.
Reprints and permissions information is available online at http://npg.nature.com/reprintsandpermissions/.

1. Kraut, D.A., Carroll, K.S. & Herschlag, D. Challenges in enzyme mechanism and energetics. *Annu. Rev. Biochem.* **72**, 517–571 (2003).
2. Henzler-Wildman, K.A. *et al.* Intrinsic motions along an enzymatic reaction trajectory. *Nature* **450**, 838–844 (2007).
3. Dai, S. *et al.* Structural snapshots along the reaction pathway of ferredoxin-thioredoxin reductase. *Nature* **448**, 92–96 (2007).
4. Mori, T., Vale, R.D. & Tomishige, M. How kinesin waits between steps. *Nature* **450**, 750–754 (2007).
5. Asbury, C.L., Fehr, A.N. & Block, S.M. Kinesin moves by an asymmetric hand-over-hand mechanism. *Science* **302**, 2130–2134 (2003).
6. Holmgren, A. Thioredoxin. *Annu. Rev. Biochem.* **54**, 237–271 (1985).
7. Lillig, C.H. & Holmgren, A. Thioredoxin and related molecules–from biology to health and disease. *Antioxid. Redox Signal.* **9**, 25–47 (2007).
8. Holmgren, A. Reduction of disulfides by thioredoxin. Exceptional reactivity of insulin and suggested functions of thioredoxin in mechanism of hormone action. *J. Biol. Chem.* **254**, 9113–9119 (1979).
9. Holmgren, A. Thioredoxin catalyzes the reduction of insulin disulfides by dithiothreitol and dihydrolipoamide. *J. Biol. Chem.* **254**, 9627–9632 (1979).
10. Holmgren, A. Tryptophan fluorescence study of conformational transitions of the oxidized and reduced form of thioredoxin. *J. Biol. Chem.* **247**, 1992–1998 (1972).
11. Wiita, A.P. *et al.* Probing the chemistry of thioredoxin catalysis with force. *Nature* **450**, 124–127 (2007).
12. Koti Ainavarapu, S.R., Wiita, A.P., Dougan, L., Uggerud, E. & Fernandez, J.M. Single-molecule force spectroscopy measurements of bond elongation during a bimolecular reaction. *J. Am. Chem. Soc.* **130**, 6479–6487 (2008).
13. Wiita, A.P., Ainavarapu, S.R., Huang, H.H. & Fernandez, J.M. Force-dependent chemical kinetics of disulfide bond reduction observed with single-molecule techniques. *Proc. Natl. Acad. Sci. USA* **103**, 7222–7227 (2006).
14. Damdimopoulos, A.E., Miranda-Vizuete, A., Pelto-Huikko, M., Gustafsson, J.A. & Spyrou, G. Human mitochondrial thioredoxin. Involvement in mitochondrial membrane potential and cell death. *J. Biol. Chem.* **277**, 33249–33257 (2002).
15. Miranda-Vizuete, A., Damdimopoulos, A.E., Gustafsson, J. & Spyrou, G. Cloning, expression, and characterization of a novel *Escherichia coli* thioredoxin. *J. Biol. Chem.* **272**, 30841–30847 (1997).
16. Spyrou, G., Enmark, E., Miranda-Vizuete, A. & Gustafsson, J. Cloning and expression of a novel mammalian thioredoxin. *J. Biol. Chem.* **272**, 2936–2941 (1997).
17. Ye, J. *et al.* Crystal structure of an unusual thioredoxin protein with a zinc finger domain. *J. Biol. Chem.* **282**, 34945–34951 (2007).
18. Boucher, I.W. *et al.* Structural and biochemical characterization of a mitochondrial peroxiredoxin from *Plasmodium falciparum*. *Mol. Microbiol.* **61**, 948–959 (2006).
19. Powis, G. & Montfort, W.R. Properties and biological activities of thioredoxins. *Annu. Rev. Biophys. Biomol. Struct.* **30**, 421–455 (2001).
20. Gelhaye, E., Rouhier, N., Navrot, N. & Jacquot, J.P. The plant thioredoxin system. *Cell. Mol. Life Sci.* **62**, 24–35 (2005).
21. Meyer, Y. *et al.* Evolution of redoxin genes in the green lineage. *Photosynth. Res.* **89**, 179–192 (2006).
22. Perez-Jimenez, R. *et al.* Force-clamp spectroscopy detects residue co-evolution in enzyme catalysis. *J. Biol. Chem.* **283**, 27121–27129 (2008).
23. Carvalho, A.T. *et al.* Mechanism of thioredoxin-catalyzed disulfide reduction. Activation of the buried thiol and role of the variable active-site residues. *J. Phys. Chem. B* **112**, 2511–2523 (2008).
24. Kappler, U. & Bailey, S. Molecular basis of intramolecular electron transfer in sulfite-oxidizing enzymes is revealed by high resolution structure of a heterodimeric complex of the catalytic molybdopterin subunit and a c-type cytochrome subunit. *J. Biol. Chem.* **280**, 24999–25007 (2005).
25. Costentin, C. & Saveant, J.M. Competition between S_N2 and single electron transfer reactions as a function of steric hindrance illustrated by the model system alkylCl + NO^-. *J. Am. Chem. Soc.* **122**, 2329–2338 (2000).
26. Holm, R.H., Kennepohl, P. & Solomon, E.I. Structural and functional aspects of metal sites in biology. *Chem. Rev.* **96**, 2239–2314 (1996).
27. McLendon, G., Komar-Panicucci, S. & Hatch, S. Applying Marcus's theory to electron transfer *in vivo*. Electron Transfer-from Isolated Molecules to Biomolecules. in *Advances in Chemical Physics* Vol 107 591–600 (John Wiley & Sons, New York, NY, 1999).
28. Erlandsson, M. & Hallbrink, M. Metallic zinc reduction of disulfide bonds between cysteine residues in peptides and proteins. *Int. J. Pept. Res. Ther.* **11**, 261–265 (2005).
29. Aslund, F., Berndt, K.D. & Holmgren, A. Redox potentials of glutaredoxins and other thiol-disulfide oxidoreductases of the thioredoxin superfamily determined by direct protein-protein redox equilibria. *J. Biol. Chem.* **272**, 30780–30786 (1997).
30. Cheng, Z., Arscott, L.D., Ballou, D.P. & Williams, C.H. Jr. The relationship of the redox potentials of thioredoxin and thioredoxin reductase from *Drosophila melanogaster* to the enzymatic mechanism: reduced thioredoxin is the reductant of glutathione in *Drosophila*. *Biochemistry* **46**, 7875–7885 (2007).
31. Yasui, S., Itoh, K., Tsujimoto, M. & Ohno, A. Irreversibility of single electron transfer occurring from trivalent phosphorus compounds to Iron(III) complexes in the presence of ethanol. *Bull. Chem. Soc. Jpn.* **75**, 1311–1318 (2002).
32. Hazzard, J.T., Marchesini, A., Curir, P. & Tollin, G. Direct measurement by laser flash photolysis of intramolecular electron transfer in the three-electron reduced form of ascorbate oxidase from zucchini. *Biochim. Biophys. Acta* **1208**, 166–170 (1994).
33. Farver, O. & Pecht, I. Low activation barriers characterize intramolecular electron transfer in ascorbate oxidase. *Proc. Natl. Acad. Sci. USA* **89**, 8283–8287 (1992).
34. Maeda, K., Hagglund, P., Finnie, C., Svensson, B. & Henriksen, A. Structural basis for target protein recognition by the protein disulfide reductase thioredoxin. *Structure* **14**, 1701–1710 (2006).
35. Li, Y. *et al.* Conformational fluctuations coupled to the thiol-disulfide transfer between thioredoxin and arsenate reductase in *Bacillus subtilis*. *J. Biol. Chem.* **282**, 11078–11083 (2007).
36. Lennon, B.W., Williams Jr., C.H., & Ludwig, M.L. Twists in catalysis: alternating conformations of *Escherichia coli* thioredoxin reductase. *Science* **289**, 1190–1194 (2000).
37. Falkowski, P.G. Evolution. Tracing oxygen's imprint on earth's metabolic evolution. *Science* **311**, 1724–1725 (2006).
38. Raymond, J. & Segre, D. The effect of oxygen on biochemical networks and the evolution of complex life. *Science* **311**, 1764–1767 (2006).
39. Kirschvink, J.L. & Kopp, R.E. Palaeoproterozoic ice houses and the evolution of oxygen-mediating enzymes: the case for a late origin of photosystem II. *Phil. Trans. R. Soc. Lond. B* **363**, 2755–2765 (2008).
40. Lemaire, S.D. *et al.* New thioredoxin targets in the unicellular photosynthetic eukaryote *Chlamydomonas reinhardtii*. *Proc. Natl. Acad. Sci. USA* **101**, 7475–7480 (2004).
41. Sharma, A. *et al.* Microbial activity at gigapascal pressures. *Science* **295**, 1514–1516 (2002).
42. La Duc, M.T. *et al.* Isolation and characterization of bacteria capable of tolerating the extreme conditions of clean room environments. *Appl. Environ. Microbiol.* **73**, 2600–2611 (2007).
43. Koch, A.L. Shrinkage of growing *Escherichia coli* cells by osmotic challenge. *J. Bacteriol.* **159**, 919–924 (1984).
44. Malone, A.S., Chung, Y.K. & Yousef, A.E. Genes of *Escherichia coli* O157:H7 that are involved in high-pressure resistance. *Appl. Environ. Microbiol.* **72**, 2661–2671 (2006).
45. Gaucher, E.A., Govindarajan, S. & Ganesh, O.K. Palaeotemperature trend for Precambrian life inferred from resurrected proteins. *Nature* **451**, 704–707 (2008).
46. Jones, P.R., Manabe, T., Awazuhara, M. & Saito, K. A new member of plant CS-lyases. A cystine lyase from *Arabidopsis thaliana*. *J. Biol. Chem.* **278**, 10291–10296 (2003).
47. Beynon, R.J., Bond, J.S. & NetLibrary Inc. Proteolytic enzymes: a practical approach. in *Practical Approach Series* 2nd edn, xviii, 340 (Oxford University Press, Oxford; New York, 2001).
48. Forman-Kay, J.D., Clore, G.M., Wingfield, P.T. & Gronenborn, A.M. High-resolution three-dimensional structure of reduced recombinant human thioredoxin in solution. *Biochemistry* **30**, 2685–2698 (1991).
49. Qin, J., Clore, G.M., Kennedy, W.M., Huth, J.R. & Gronenborn, A.M. Solution structure of human thioredoxin in a mixed disulfide intermediate complex with its target peptide from the transcription factor NF kappa B. *Structure* **3**, 289–297 (1995).
50. Peterson, F.C. *et al.* Solution structure of thioredoxin h1 from *Arabidopsis thaliana*. *Protein Sci.* **14**, 2195–2200 (2005).
51. Capitani, G. *et al.* Crystal structures of two functionally different thioredoxins in spinach chloroplasts. *J. Mol. Biol.* **302**, 135–154 (2000).
52. Smeets, A. *et al.* Crystal structures of oxidized and reduced forms of human mitochondrial thioredoxin 2. *Protein Sci.* **14**, 2610–2621 (2005).
53. Katti, S.K., LeMaster, D.M. & Eklund, H. Crystal structure of thioredoxin from *Escherichia coli* at 1.68 resolution. *J. Mol. Biol.* **212**, 167–184 (1990).
54. Lancelin, J.M., Guilhaudis, L., Krimm, I., Blackledge, M.J., Marion, D. & Jacquot, J.P. NMR structures of thioredoxin *m* from the green alga *Chlamydomonas reinhardtii*. *Proteins* **41**, 334–349 (2000).
55. Qin, J., Clore, G.M., Kennedy, W.P., Kuszewski, J. & Gronenborn, A.M. The solution structure of human thioredoxin complexed with its target from Ref-1 reveals peptide chain reversal. *Structure* **4**, 613–620 (1996).

ONLINE METHODS

Protein expression and purification. Preparation of $(I27_{G32S-A75C})_8$ polyprotein has been described extensively[11,22]. The expression and purification of the different Trxs used have also been described: *P. falciparum*[56], *Drosophila melanogaster* Trx1 (ref. 57), poplar Trxh1 (ref. 58) and Trx*h*3 (ref. 59), pea Trx*m*[60], *E. coli* Trx1 (ref. 61), *E. coli* Trx2 (ref. 17) and human TRX2 (ref. 14).

Sequence analysis. We carried out sequence alignment using ClustalW and modified by hand. Tree topology and branch lengths of the tree were estimated using Mr. Bayes (v. 3.5) (http://mrbayes.csit.fsu.edu/), with rate variation modeled according to a gamma distribution. The following GI numbers were accessed from GenBank. Bacteria: *E. coli* Trx1 (67005950), *Salmonella* Trx1 (16767191), *E. coli* Trx2 (16130507), *Salmonella* Trx2 (16765969), human TRX2 mitochondria (21361403), bovine Trx2 mitochondria (108935910), *Rickettsia* Trx (15603883), *Nostoc* Trx (17227548), *Proclorococcus* Trx (126696505), spinach Trx*m* chloroplast (2507458), pea Trx*m* chloroplast (1351239), *Thermus* Trx (46199687), *Deinococcus* Trx (15805968), Archaea *Aeropyrum* Trx (118431868), *Hyperthermus* Trx (124027987), *Sulfolobus* Trx (15897303). Eukaryote: *P. falciparum* Trx (75024181), poplar Trx*h*1 (19851972), poplar Trx*h*3 (2398305), pea Trx (27466894), *Dictyostelium* Trx (165988451), bovine Trx (27806783), human TRX1 (135773).

Single-molecule force-clamp experiments. The details of our custom-made atomic force microscope have been described previously[62]. We used silicon nitride cantilever (Veeco) with a typical spring constant of 20 pN nm^{-1}, calibrated using the equipartition theorem. The force-clamp mode provides an extension resolution of ~0.5 nm and a piezoelectric actuator feedback of ~5 ms. The buffer used in all the experiments was 10 mM HEPES, 150 mM NaCl, 1mM EDTA, 2mM NADPH at pH 7.2. Before the beginning of the experiment, TrxR, bacterial or eukaryotic depending on the case, was added to a final concentration of 50 nM. The different Trxs were added to the desired concentration. The reaction mixture and the substrate were added and allowed to absorb onto a freshly evaporated gold coverslip before the experiments. The force-clamp experiment consisted of a double-pulse force protocol. The first pulse was set at 175 pN during 0.3–0.4 s. The second pulse can be set at different forces and was held long enough to capture all the possible reduction events. We carried out the experiments using metallic zinc in 100 mM citrate buffer at pH 6. After adding zinc nanoparticles (Sigma) to a concentration of 10 mM, we sonicated the solution to allow resuspension. The pH of the buffer was verified during the time of the experiment, and no appreciable changes were observed. In addition, to verify the behavior of the substrate in citrate buffer, we carried out several control experiments in the absence of zinc nanoparticles and detected no reduction events. We collected and analyzed data using custom-written software in IGOR Pro 6.03 (Wavemetrics). The collected traces (15–50 per force) containing the reduction events were summated and averaged. The resulting averaged traces were fit with a single exponential from which the rate constant was obtained. We analyzed the force-dependent reduction kinetics using the kinetic model in the **Supplementary Methods**.

56. Kanzok, S.M., Schirmer, R.H., Turbachova, I., Iozef, R. & Becker, K. The thioredoxin system of the malaria parasite *Plasmodium falciparum*. Glutathione reduction revisited. *J. Biol. Chem.* **275**, 40180–40186 (2000).
57. Kanzok, S.M. *et al.* Substitution of the thioredoxin system for glutathione reductase in *Drosophila melanogaster*. *Science* **291**, 643–646 (2001).
58. Behm, M. & Jacquot, J.P. Isolation and characterization of thioredoxin *h* from poplar xylem. *Plant Physiol. Biochem.* **38**, 363–369 (2000).
59. Gelhaye, E. *et al.* Identification and characterization of a third thioredoxin *h* in poplar. *Plant Physiol. Biochem.* **41**, 629–635 (2003).
60. López Jaramillo, J. *et al.* High-yield expression of pea thioredoxin *m* and assessment of its efficiency in chloroplast fructose-1,6-bisphosphatase activation. *Plant Physiol.* **114**, 1169–1175 (1997).
61. Perez-Jimenez, R., Godoy-Ruiz, R., Ibarra-Molero, B. & Sanchez-Ruiz, J.M. The efficiency of different salts to screen charge interactions in proteins: a Hofmeister effect? *Biophys. J.* **86**, 2414–2429 (2004).
62. Fernandez, J.M. & Li, H.B. Force-clamp spectroscopy monitors the folding trajectory of a single protein. *Science* **303**, 1674–1678 (2004).

doi:10.1038/nsmb.1627